AIAA JOURNAL
Vol. 47, No. 8, August 2009

Fracture Mechanics Analysis of Composite Structures Using the Boundary Element Shape Sensitivities

Azam Tafreshi*
University of Manchester, Manchester, England M60 1QD, United Kingdom

DOI: 10.2514/1.41729

Based on the shape sensitivity analysis of multiregion domains using the boundary element method, stress intensity factors of the cracks of arbitrary geometric shapes in anisotropic elastic solids are calculated. The results obtained agree very well with the existing analytical or numerical solutions. In contrast to the *J*-integral method, which would require the computation of stresses and strains at a series of internal points around the crack for evaluation of the path-independent integrals, the fracture mechanics parameters are evaluated here by direct differentiation of the structural response for a multiregion domain. Therefore, the present method is computationally more accurate and efficient. The length of the crack of arbitrary geometric shape is treated as the shape design variable. Then the shape variable is associated with the coordinates of a series of boundary nodes located on the crack surface. Thus, the relevant velocity terms are applied together in the sensitivity analysis with respect to that variable to determine the energy release rate, which is the total derivative of the strain energy with respect to crack length. Five example problems with anisotropic material properties are presented to validate the applications of this formulation. The results show that although the stress intensity factor is of fundamental importance in the prediction of brittle failure using linear elastic fracture mechanics, the direct evaluation of the strain energy release rate would easily characterize the crack instability of a loaded laminated composite for different fiber orientations. The results show that the strain energy release rate is highly influenced by the fiber orientation of the composite lamina. Therefore, a laminate can be tailored to crack-growth resistance.

Nomenclature

A_{jk}	=	complex constants
a	=	crack length
a_{jk}	=	elastic compliance matrix ($j, k = 1, 2, 6$)
a_{11}	=	$1/E_1$
a_{12}	=	$-(\nu_{12}/E_1)$ and $-(\nu_{21}/E_2)$
a_{16}	=	$\eta_{12,1}/E_1$ and $\eta_{1,12}/G_{12}$
a_{22}	=	$1/E_2$
a_{26}	=	$\eta_{12,2}/E_2$ and $\eta_{2,12}/G_{12}$
a_{66}	=	$1/G_{12}$
C	=	ratio of relative displacements
$C_{jk}(P)$	=	limiting value of the surface integral of $T_{jk}(P, Q)$
D_s	=	operator ($s = 1, 4$)
E_k	=	Young's modulus in the x_k direction
E_s	=	elastic compliance
F	=	ratio of stress intensity factors
G_{12}	=	shear modulus
$J(\xi)$	=	Jacobian of transformation from global Cartesian coordinates to intrinsic coordinates of the element
J_k	=	J integral ($k = 1, 2$)
$K_{\mathrm{I}}, K_{\mathrm{II}}$	=	modes I and II stress intensity factors
m_{1k}, m_{2k}	=	unit vectors tangent and normal to the surface
$N^c(\xi)$	=	quadratic shape function corresponding to the cth node of the element
n_1, n_2	=	direction cosines of the unit outward normal vector to the surface of the elastic body
P	=	load point at the surface of the elastic domain
Q	=	field point at the surface of the elastic domain
r_{jk}	=	complex constants
s	=	domain boundary
s_b	=	bth element of the discretized boundary
s_j	=	material property parameters
$T_{jk}(P, Q)$	=	jth component of the traction vector at point Q due to a unit point load in the kth direction at P
t_j	=	traction vector
U_{jk}	=	jth component of the displacement vector at point Q due to a unit point load in the kth direction at P
u_j	=	displacement vector
W	=	strain energy density
x_i	=	rectangular Cartesian coordinates
$\bar{x}_1, \bar{x}_2$	=	local coordinates on an element
z_j	=	complex coordinates
α_j, β_j	=	real constants
δ_{jk}	=	Kronecker delta
δ_1, δ_2	=	relative sliding and opening displacements
ζ_{I}	=	coordinates of the load point
$\eta_{jk,1}, \eta_{1,jk}$	=	coefficients of mutual influence of the first and second kind, respectively
Λ_1, Λ_2	=	real functions of the Cartesian and intrinsic coordinates at each integration point
μ_s	=	roots of the characteristic equation
ν_{jk}	=	Poisson's ratio
ξ	=	intrinsic coordinates of the isoparametric quadratic element
σ_{jk}	=	stress tensor
ϕ	=	airy stress function
φ	=	crack orientation angle
ψ	=	fiber orientation angle
Ω_1, Ω_2	=	real functions of the Cartesian and intrinsic coordinates at each integration point
ω	=	shape variable such as crack length

Received 20 October 2008; revision received 25 April 2009; accepted for publication 27 April 2009.

*Academic Staff, School of Mechanical, Aerospace and Civil Engineering, P.O. Box 88, Sackville Street; azam.tafreshi@manchester.ac.uk.

I. Introduction

THE application of composites in aerospace, automobile, civil, and marine industries is well established today, due to the known benefits such as high specific stiffness or strength and the material's tailoring facilities for creating high-performance structures. With the increasing need to produce lighter-weight aerospace structures, the use of advanced composite materials has become more

common in the design of these structures. Military and civilian aircraft structures are prone to cracking due to wear and tear, especially when they are used beyond their fatigue life. Cracked structures on an aircraft could lead to a catastrophic failure, because the tensile strengths of composite laminates are significantly reduced when stress concentrations such as cracks and cutouts are present. Solutions to these problems in anisotropic elasticity are therefore of great interest in the design and strength analysis of composite structures [1–11]. The finite element (FE) and boundary element (BE) are the most extensively used methods for the analysis of engineering structures. The latter seems to have proved advantageous for solving fracture mechanics problems. Early contribution to the development of the boundary element method (BEM) for cracked anisotropic plates belongs to Snyder and Cruse [1].

For problems containing a crack tip in linear elasticity, the mixed-mode singular near-tip stress field can be characterized by a pair of stress intensity factors (SIFs). For isotropic materials, SIFs have been used to predict fatigue crack growth and fracture. Several methods are available to extract the SIF and hence the strain energy release rate (SERR) [12]. Generally, the most useful way to predict the behavior of a cracked body is using the J-integral method [13]. The J integral is path-independent for all integral paths surrounding the crack tip. Using this method would require the computation of stresses and strains at a series of internal points around the crack, for evaluation of the path-independent integrals, which is obviously time-consuming.

For elastic problems, the J_1 integral is the energy release rate per unit extension of the crack. In conjunction with the finite element method (FEM) or BEM, it is possible to use the shape sensitivity analysis to directly evaluate the sensitivity of the total strain energy in which the crack length is being treated as the shape variable. This approach has been used by a few researchers [14–16] who have mainly studied the line cracks in homogeneous and isotropic materials. However, in conjunction with the FEM, Reddy and Rao [16] used the continuum shape sensitivity analysis of a mixed-mode fracture in functionally graded materials using the FEM.

Shape sensitivity analysis, which is the calculation of quantitative information on how the response of a structure is affected by changes in the variables that define its shape, is a fundamental requirement for shape optimization. Shape optimization is an important area of current development in mechanical and structural design. Computerized procedures using optimization algorithms can iteratively determine the optimum shape of a component while satisfying some objectives, without violating the design constraints at the same time. The BEM, being a surface-oriented technique, is well suited for shape optimization problems (in particular, shape sensitivity analysis).

In [17], a directly differentiated form of the boundary integral equation (BIE), with respect to boundary-point coordinates, was used to calculate stress and displacement derivatives for 2-D anisotropic structures. In [18], the optimal shape design of an anisotropic elastic body of maximum stiffness and minimum weight, under specified loadings and using the BEM, was obtained. Using the sensitivities of the elastic compliance, the stiffness of the structure was minimized and constraints were placed on the maximum stress and weight. The objective of the work in [19] is directed toward the optimal positioning of features in anisotropic structures for maximum stiffness, whereas the weight remains unchanged. For this purpose, the design sensitivity analysis with respect to the translation and rotation of the voids of arbitrary shapes using the BEM was performed. In [20], the shape sensitivity analysis of composite structures in contact has been carried out by direct differentiation of the structural response, rather than using the finite difference method. The design variables are taken as the coordinates of some nodes on the boundaries of the bodies that are in contact. The selection of the boundary points as the design variables is more general than selecting simple geometrical variables such as radii. The advantage of the proposed method is that it can be applied to any geometry, not just regular shapes. However, when entire segments of the boundary or domain are governed by a single variable such as radius, the relevant velocity terms are applied together in the sensitivity analysis with respect to this variable [19]. The results show the influence of the material properties on the sensitivities of the contact pressure and strain energy of the anisotropic components in contact. To the author's knowledge, no other publications are available on the shape optimization or sensitivities of composite materials using the boundary elements.

This paper presents the application of the boundary element shape sensitivity for the analysis of two-dimensional anisotropic bodies with cracks of arbitrary shapes. The design sensitivity analysis of multiregion domains with anisotropic material properties has been carried out by direct differentiation of the structural response. The length of the crack of arbitrary shape is treated as the shape variable. The shape variable is then associated with the coordinates of a series of boundary nodes located on the crack surfaces. Thus, the relevant velocity terms are applied together in the sensitivity analysis with respect to that variable to determine the derivatives of displacements and stresses and the elastic compliance of the structure with respect to the crack extension. Following the calculation of the rate of energy released per unit of crack extension and the related material property parameters of a composite material, the SIFs of the structure in single- or mixed-mode loading conditions are determined. This paper shows the advantage of using the boundary element shape sensitivities in crack analysis over the J-integral method, both in terms of the computational modeling and numerical accuracy.

The study on instability analysis of delaminated composite cylindrical shells subject to axial compression, external pressure, and bending, either applied individually or in combination [21–23], showed that the SERR was more convenient to use for the prediction of crack growth and fracture of delaminated composite structures. Here, it is shown that although the SIF is of fundamental importance in the prediction of brittle failure using linear elastic fracture mechanics, the SERR for cracked anisotropic meshes has been found to be more convenient for these predictions. Five example problems with anisotropic material properties are presented to validate the applications of this formulation. The results show good agreement with results reported in the literature.

II. Constitutive Equations for Plane Anisotropic Elasticity

Combining the stress–strain relations, the compatibility equation of strains, and the equilibrium equation, the governing equation for the two-dimensional problem of homogeneous and anisotropic elasticity can be obtained [24]:

$$a_{22}\frac{\partial^4\phi}{\partial x_1^4} - 2a_{26}\frac{\partial^4\phi}{\partial x_1^3\partial x_2} + (2a_{12}+a_{66})\frac{\partial^4\phi}{\partial x_1^2\partial x_2^2} - 2a_{16}\frac{\partial^4\phi}{\partial x_1\partial x_2^3} + a_{66}\frac{\partial^4\phi}{\partial x_2^4} = 0 \tag{1}$$

The coefficients a_{jk} are the elastic compliances of the material. For especially orthotropic materials, $a_{16} = a_{26} = a_{63} = 0$ [25]. By introducing the operator $D_s (s = 1, 4)$ as

$$D_s = \frac{\partial}{\partial x_2} - \mu_s \frac{\partial}{\partial x_1} \tag{2}$$

Eq. (1) becomes

$$D_1 D_2 D_3 D_4(\phi) = 0 \tag{3}$$

and μ_s are the four roots of the characteristic equation:

$$[a_{22} - 2\mu a_{26} + (2a_{12}+a_{66})\mu^2 - 2a_{16}\mu^3 + a_{11}\mu^4]\frac{d^4\phi}{dz^4} = 0 \tag{4}$$

To have a solution for the stress function, the term in square brackets must be zero. Lehknitskii [25] has shown that for an anisotropic material, these roots are distinct and must be purely imaginary or complex and they may be denoted by

$$\mu_1 = \alpha_1 + i\beta_1, \qquad \mu_1 = \alpha_2 + i\beta_2, \qquad \mu_3 = \bar{\mu}_1, \qquad \mu_4 = \bar{\mu}_2 \tag{5}$$

where α_j and $\beta_j (j = 1, 2)$ are real constants, $i = \sqrt{-1}$, and the overbar represents the complex conjugate. Therefore, the stresses and displacements in an anisotropic body can be expressed in terms of the complex coordinates z_j,

$$z_j = x_1 + \mu_j x_2 \qquad j = 1, 2 \tag{6}$$

and their complex conjugates.

III. Anisotropic Fracture Mechanics

The SIF is of fundamental importance in the prediction of brittle failure using linear elastic fracture mechanics. It is a function of both the cracked geometry and the associated loading. $K_{\mathrm{I}}$and K_{II} are the mode I and mode II SIFs, respectively. They characterize the stress fields in the vicinity of the crack tip with respect to a local Cartesian (x_1–x_2) system that has its origin at the tip of the crack and is oriented with the angle of φ with respect to the global Cartesian system (x–y) (see Fig. 1).

The J-integral method was first developed by Rice [13] to characterize fracture for two-dimensional configurations modeled by a linear or nonlinear elastic material. For such a material of unit thickness containing a traction free crack, the J_k integral is defined as

$$J_k = \oint_c (W n_k - t_i u_{j,k}) ds \tag{7}$$

where $j, k = 1, 2$, W is the strain energy density, S is a generic contour surrounding the crack tip, $t_{i=}\sigma_{ij} n_i$ are the traction components defined along the contour, and n_i are the components of the unit outward normal to the contour path, as shown in Fig. 1. The J_1 integral is Rice's path-independent integral. Using the J-integral method, a circular path may be generated with the center at the crack tip, defining the number of internal points to be computed, beginning on one crack face and finishing on the other. With the numerical integration of Eq. (7), J_1 can then be determined.

J_1 is also equal to the rate of energy released per unit of crack extension along the x_1 axis. If the length of the crack of arbitrary shape is treated as the shape design variable, then the SERR that is the derivative of the elastic compliance of the structure with respect to the crack length extension is evaluated by direct differentiation of the BIE.

The J_1 integral is related to the SIFs of a cracked homogeneous anisotropic plate by [6]

$$J_1 = \alpha'_{11} K_{\mathrm{I}}^2 + \alpha'_{12} K_{\mathrm{I}} K_{\mathrm{II}} + \alpha'_{22} K_{\mathrm{II}}^2 \tag{8}$$

where

$$\begin{aligned} \alpha'_{11} &= -\frac{a'_{22}}{2} \operatorname{Im}\left(\frac{s_1 + s_2}{s_1 s_2}\right), \qquad \alpha'_{22} = \frac{a'_{11}}{2} \operatorname{Im}(s_1 + s_2), \\ \alpha'_{12} &= -\frac{a'_{22}}{2} \operatorname{Im}\left(\frac{1}{s_1 s_2}\right) + \frac{a'_{11}}{2} \operatorname{Im}(s_1 s_2) \end{aligned} \tag{9}$$

In Eqs. (9), s_1 and s_2 are the material property parameters that are related to the roots of the characteristic equation (4) as follows:

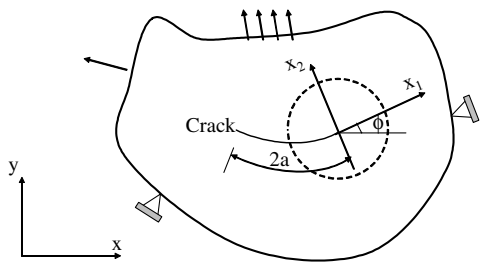

Fig. 1 General crack body under mixed-mode loading.

$$s_j = \frac{\mu_j \cos\varphi + \sin\varphi}{\cos\varphi - \mu_j \sin\varphi} \qquad j = 1, 2 \tag{10}$$

where $a'_{ij}s$ are the compliance constants obtained from the transformation of a_{jk} from the global system to the local coordinate system, as follows [7]:

$$\begin{aligned} a'_{11} &= a_{11}\cos^4\varphi + (2a_{12} + a_{66})\sin^2\varphi\cos^2\varphi + a_{22}\sin^4\varphi \\ &\quad + (a_{16}\cos^2\varphi + a_{26}\sin^2\varphi)\sin 2\varphi \\ a'_{22} &= a_{11}\sin^4\varphi + (2a_{12} + a_{66})\sin^2\varphi\cos^2\varphi + a_{22}\cos^4\varphi \\ &\quad - (a_{16}\cos^2\varphi + a_{26}\sin^2\varphi)\sin 2\varphi \\ a'_{12} &= a_{12} + (a_{11} + a_{22} - 2a_{12} - a_{66})\sin^2\varphi\cos^2\varphi \\ &\quad + \tfrac{1}{2}(a_{26} - a_{16})\sin 2\varphi\cos 2\varphi \\ a'_{66} &= a_{66} + 2(a_{11} + a_{22} - 2a_{12} - a_{66})\sin^2 2\varphi \\ &\quad + 2(a_{26} - a_{16})\sin 2\varphi\cos 2\varphi \\ a'_{16} &= \left[a_{22}\sin^2\varphi - a_{11}\cos^2\varphi + \frac{1}{2}(2a_{12} + a_{66})\cos 2\varphi\right]\sin 2\varphi \\ &\quad + (a_{16}\cos^2\varphi)(\cos^2\varphi - 3\sin^2\varphi) + (a_{26}\sin^2\varphi)(3\cos^2\varphi - \sin^2\varphi) \\ a'_{26} &= \left[a_{22}\cos^2\varphi - a_{11}\sin^2\varphi - \frac{1}{2}(2a_{12} + a_{66})\cos 2\varphi\right]\sin 2\varphi \\ &\quad + (a_{16}\sin^2\varphi)(3\cos^2\varphi - \sin^2\varphi) + (a_{26}\cos^2\varphi)(\cos^2\varphi - 3\sin^2\varphi) \end{aligned} \tag{11}$$

For isotropic materials, $\alpha'_{11} = \alpha'_{22} = 1/E$ and $\alpha'_{12} = 0$; therefore,

$$J_1 = \frac{K_{\mathrm{I}}^2 + K_{\mathrm{II}}^2}{E} \tag{12}$$

For decoupling of K_{I} and K_{II}, an auxiliary relationship in terms of displacements ratio can be developed to be used together with J_1. The displacements on the crack surface ($\theta = \pm\pi$) near the crack tip of a two-dimensional anisotropic body may be written in the form [8]

$$\begin{bmatrix} u_1 \\ u_2 \end{bmatrix} = \sqrt{\frac{2r}{\pi}} \begin{bmatrix} D_{11} & D_{12} \\ D_{21} & D_{22} \end{bmatrix} \begin{bmatrix} K_{\mathrm{I}} \\ K_{\mathrm{II}} \end{bmatrix} \tag{13}$$

where

$$\begin{aligned} D_{11} &= \operatorname{Im}\left(\frac{s_2 r'_{11} - s_1 r'_{12}}{s_1 - s_2}\right), \qquad D_{12} = \operatorname{Im}\left(\frac{r'_{11} - r'_{12}}{\mu_1 - \mu_2}\right) \\ D_{21} &= \operatorname{Im}\left(\frac{s_2 r'_{21} - s_1 r'_{22}}{s_1 - s_2}\right), \qquad D_{22} = \operatorname{Im}\left(\frac{r'_{21} - r'_{22}}{s_1 - s_2}\right) \end{aligned} \tag{14}$$

which shows the coupling of K_{I} and K_{II} for mixed-mode problems in anisotropic bodies, and r'_{ij} is defined as follows:

$$r'_{1j} = a'_{11} s_j^2 + a'_{12} - a'_{16} s_j, \qquad r'_{2j} = a'_{12} s_j + a'_{22}/s_j - a'_{26} \tag{15}$$

If δ_1 and δ_2 are the relative sliding and opening displacements for $\theta = \pm\pi$, respectively, then

$$\delta_1 = 2\sqrt{\frac{2r}{\pi}}(D_{11} K_{\mathrm{I}} + D_{12} K_{\mathrm{II}}), \qquad \delta_2 = 2\sqrt{\frac{2r}{\pi}}(D_{21} K_{\mathrm{I}} + D_{22} K_{\mathrm{II}}) \tag{16}$$

The ratio of relative displacements is

$$C = \frac{\delta_2}{\delta_1} = \frac{D_{21} K_{\mathrm{I}} + D_{22} K_{\mathrm{II}}}{D_{11} K_{\mathrm{I}} + D_{12} K_{\mathrm{II}}} \tag{17}$$

and the ratio of stress intensity factors

$$F = \frac{K_{\mathrm{I}}}{K_{\mathrm{II}}} = \frac{C D_{12} - D_{22}}{D_{21} - C D_{11}} \tag{18}$$

or

$$K_{\mathrm{I}} = FK_{\mathrm{II}} \tag{19}$$

Once J_1 or the derivative of the strain energy with respect to the crack length extension is obtained, then K_{II} can be obtained by substituting Eq. (19) into Eq. (8):

$$K_{\mathrm{II}} = \left(\frac{J_1}{\alpha'_{11}F^2 + \alpha'_{12}F + \alpha'_{22}}\right)^{1/2} \tag{20}$$

IV. Review of the Boundary Element Method for Anisotropic Elasticity

The analytical formulation of the direct BIE for plane anisotropic elasticity may be developed by following the same steps as in the isotropic case [3].

The BEM is based on the unit load solutions in an infinite body, known as the fundamental solutions, used with the reciprocal work theorem and appropriate limit operations. The BIE of the anisotropic materials is an integral constraint equation relating boundary tractions t_j and boundary displacements u_j and it may be written as

$$C_{jk}u_j(P) + \int_s T_{jk}(P,Q)u_j(Q)\mathrm{d}s(Q) = \int_s U_{jk}(P,Q)t_j(Q)\mathrm{d}s(Q) \qquad j,k = 1,2 \tag{21}$$

where $P(\zeta_1, \zeta_2)$ and $Q(x_1, x_2)$ are the field and load points, respectively; $U_{jk}(P,Q)$ and $T_{jk}(P,Q)$ are the fundamental solutions that represent the displacements and tractions, respectively, in the x_k direction at Q because of a unit load in the x_j direction at P in an infinite body; and the constant C_{jk} depends on the local geometry of the boundary at P, whether it lies on a smooth surface or a sharp corner. In terms of the generalized complex variables

$$z_1 = (x_1 - \zeta_1) + \mu_1(x_2 - \zeta_2) \qquad z_2 = (x_1 - \zeta_1) + \mu_2(x_2 - \zeta_2) \tag{22}$$

the fundamental solutions for displacements and tractions, respectively, can be written as

$$\begin{aligned} U_{jk} &= 2\mathrm{Re}[r_{k1}A_{j1}\ell_n(z_1) + r_{k2}A_{j2}\ell_n(z_2)] \\ T_{j1} &= 2n_1\mathrm{Re}[\mu_1^2A_{j1}/z_1 + \mu_2^2A_{j2}/z_2] - 2n_2\mathrm{Re}[\mu_1A_{j1}/z_1 + \mu_2A_{j2}/z_2] \\ T_{j2} &= -2n_1\mathrm{Re}[\mu_1A_{j1}/z_1 + \mu_2A_{j2}/z_2] + 2n_2\mathrm{Re}[A_{j1}/z_1 + A_{j2}/z_2] \end{aligned} \tag{23}$$

where n_j are the unit outward normal components at Q with respect to the x_1–x_2 coordinate system. The constants r_{kj} are

$$r_{1j} = a_{11}\mu_j^2 + a_{12} - a_{16}\mu_j, \qquad r_{2j} = a_{12}\mu_j + a_{22}/\mu_j - a_{26} \tag{24}$$

and A_{jk} are complex constants that can be obtained from the following set of equations:

$$\begin{aligned} A_{j1} - \bar{A}_{j1} + A_{j2} - \bar{A}_{j2} &= \delta_{j2}/2\pi i \\ \mu_1A_{j1} - \bar{\mu}_1\bar{A}_{j1} + \mu_2A_{j2} - \bar{\mu}_2\bar{A}_{j2} &= -\delta_{j1}/2\pi i \\ r_{11}A_{j1} - \bar{r}_{11}\bar{A}_{j1} + r_{21}A_{j2} - \bar{r}_{21}\bar{A}_{j2} &= 0 \\ r_{12}A_{j1} - \bar{r}_{12}\bar{A}_{j1} + r_{22}A_{j2} - \bar{r}_{22}\bar{A}_{j2} &= 0 \end{aligned} \tag{25}$$

An elastic body with several cracks may be divided into several subregions in which the crack faces coincide with the boundaries of the subregions. The multiregion modeling approach was first exploited for crack modeling by Blandford et al. [26], in which BIE [Eq. (21)] is employed individually for each subregion L in turn:

$$C_{jk}^{(L)}u_j^{(L)}(P) + \int_{s(L)} T_{jk}^{(L)}(P,Q)u_j^{(L)}(Q)\mathrm{d}s^{(L)}(Q) = \int_s U_{jk}^{(L)}(P,Q)t_j^{(L)}(Q)\mathrm{d}s^{(L)}(Q) \qquad j,k = 1,2 \tag{26}$$

The boundary element implementation of Eq. (26) entails boundary discretization. Quadratic isoparametric elements can be employed for the analyses. Substitution of these isoparametric representations into Eq. (26) will result in a set of linear algebraic equations for the unknown displacements and tractions at the nodes on the boundary of the solution domain as follows:

$$AU = B \tag{27}$$

where A is the final coefficient matrix, U is a vector containing the unknown displacements or tractions, and the second member B is a vector that consists of all the known values multiplied by corresponding matrix elements. Then appropriate continuity and equilibrium conditions are applied at the common subregion interface before the linear algebraic equations are solved. For example, for two subregions, R_a and R_b, respectively,

$$u_i^{Ra} = u_i^{Rb}, \qquad t_i^{Ra} + t_i^{Rb} = 0 \tag{28}$$

V. Sensitivities of the Structural Response for a Multiregion Domain

In a recent study by the author [20], a directly differentiated form of BIE with respect to geometric design variables was used to calculate shape design sensitivities for anisotropic materials with frictionless contact. The selected design variables were the coordinates of the boundary points either in the contact or noncontact area. The selection of the boundary points as the design variables was more general than selecting simple geometrical variables such as radii, etc. The advantage of the proposed method was that it can be applied to any geometry, not necessarily regular shapes. However, when entire segments of the boundary or domain were governed by a single variable such as radius, the relevant velocity terms were applied together in the sensitivity analysis with respect to that variable [19] to determine the gradients of the objective function and the constraints. It was shown that if the entire boundary is governed by a single geometric variable ω, such as radius, the material derivative F' with respect to the variable can be written as

$$\frac{dF}{d\omega} = \frac{\partial F}{\partial \omega} + \frac{\partial F}{\partial x_i}\frac{\partial x_i}{\partial \omega} \tag{29}$$

where $\partial F/\partial\omega$ is equal to zero because the shape variables are not explicit terms in the BIE; $\partial F/\partial x_i$ are derivatives of the function F with respect to the coordinates of the nodes located on the boundary; $\partial x_i/\partial\omega$ can be obtained by the definition of appropriate relations between the boundary-point coordinates and the geometric variable ω; and the function F can be the elastic compliance of the structure, contact stress, displacement, etc.

Here, using a similar approach, the crack length of arbitrary geometric shape is selected as the shape design variable. Then the shape variable is associated with the coordinates of a series of boundary nodes located on the crack surface. Thus, the relevant velocity terms are applied together in the sensitivity analysis with respect to that variable to determine the gradients of the elastic compliance or the SERR with respect to the crack length extension. The following shows how the sensitivities of displacements, stresses, and elastic compliance with respect to the boundary-point coordinates for a multiregion domain are calculated.

Direct differentiation of the BIE for each subregion with respect to a design variable x_h ($h = 1, 2$) (which is most likely to be the coordinate of a node on the crack surface) results in the following equation:

$$C_{jk}^{(L)}\frac{\partial u_j^{(L)}(P)}{\partial x_h}+\frac{\partial C_{jk}^{(L)}}{\partial x_h}u_j^{(L)}(P)+\int_{s(L)}\left[\frac{\partial T_{jk}^{(L)}(P,Q)}{\partial x_h}u_j^{(L)}(Q)+T_{jk}^{(L)}(P,Q)\frac{\partial u_j^{(L)}(Q)}{\partial x_h}\right]\mathrm{d}s^{(L)}(Q)+\int_{s(L)}[T_{jk}^{(L)}(P,Q)u_j^{(L)}(Q)]$$
$$\frac{\partial[\mathrm{d}s^{(L)}(Q)]}{\partial x_h}=\int_{s(L)}\left[\frac{\partial U_{jk}^{(L)}(P,Q)}{\partial x_h}t_j^{(L)}(Q)+U_{jk}^{(L)}(P,Q)\frac{\partial t_j^{(L)}(Q)}{\partial x_h}\right]$$
$$\times\mathrm{d}s^{(L)}(Q)\int_s U_{jk}^{(L)}(P,Q)t_j^{(L)}(Q)\frac{\partial[\mathrm{d}s^{(L)}(Q)]}{\partial x_h}\quad j,k=1,2 \tag{30}$$

The derivatives of the terms that only depend on the geometry will be carried out similarly to the isotropic materials [27]. The derivatives of the kernels for anisotropic materials will be as follows [17]:

$$\frac{\partial U_{jk}}{\partial x_h}=2\frac{\partial}{\partial x_h}[\mathrm{Re}(r_{k1}A_{j1}\,\ell_n(z_1)+r_{k2}A_{j2}\,\ell_n(z_2))]$$
$$\frac{\partial T_{j1}}{\partial x_h}=2n_1\frac{\partial}{\partial x_h}\left[\mathrm{Re}\left(\frac{\mu_1^2A_{j1}}{z_1}+\frac{\mu_2^2A_{j2}}{z_2}\right)\right]+2\,\mathrm{Re}\left(\frac{\mu_1^2A_{j1}}{z_1}+\frac{\mu_2^2A_{j2}}{z_2}\right)\frac{\partial(n_1)}{\partial x_h}-2n_2\frac{\partial}{\partial x_h}\times\left[\mathrm{Re}\left(\frac{\mu_1A_{j1}}{z_1}+\frac{\mu_2A_{j2}}{z_2}\right)\right]-2\,\mathrm{Re}\left(\frac{\mu_1A_{j1}}{z_1}+\frac{\mu_2A_{j2}}{z_2}\right)\frac{\partial(n_2)}{\partial x_h}$$
$$\frac{\partial T_{j2}}{\partial x_h}=-2n_1\frac{\partial}{\partial x_h}\left[\mathrm{Re}\left(\frac{\mu_1A_{j1}}{z_1}+\frac{\mu_2A_{j2}}{z_2}\right)\right]-2\,\mathrm{Re}\left(\frac{\mu_1A_{j1}}{z_1}+\frac{\mu_2A_{j2}}{z_2}\right)\frac{\partial(n_1)}{\partial x_h}+2n_2\frac{\partial}{\partial x_h}\left[\mathrm{Re}\left(\frac{A_{j1}}{z_1}+\frac{A_{j2}}{z_2}\right)\right]+2\,\mathrm{Re}\left(\frac{A_{j1}}{z_1}+\frac{A_{j2}}{z_2}\right)\frac{\partial(n_2)}{\partial x_h} \tag{31}$$

The coefficients m_j and A_{jk} depend on the material properties and are independent of the boundary-node coordinates. To calculate the preceding derivatives, the complex values $\ell_n(z_j)$ and $1/z_j$ can be written as

$$\ell_n(z_j)=\ell_n|z_j|+i\arg(z_j),\qquad \frac{1}{z_j}=\frac{\bar{z}_j}{|z_j|^2} \tag{32}$$

Defining the real functions Λ_j and Ω_j as

$$\Lambda_1=(x_1-\zeta_1)+\alpha_1(x_2-\zeta_2),\qquad \Lambda_2=(x_1-\zeta_1)+\alpha_2(x_2-\zeta_2)$$
$$\Omega_1=-\beta_1\zeta_2+\beta_1x_2,\qquad \Omega_2=-\beta_2\zeta_2+\beta_2x_2 \tag{33}$$

The complex coordinates and their conjugates can be written as

$$z_j=\Lambda_j+i\Omega_j,\qquad \bar{z}_j=\Lambda_j-i\Omega_j \tag{34}$$

By substituting Eqs. (32–34) into Eqs. (31), the derivatives of the kernel products with respect to the design variable x_h can be obtained.

For calculation of the sensitivities of an elastic body that is divided into several subregions, the boundary constraints [Eq. (28)] must be differentiated with respect to the design variable. The differentiated form of the boundary constraints will create relationships between the derivatives of the displacements and tractions of the node pairs. For the stick node pair (Na and Nb), the differentiated form of Eq. (28) is

$$\frac{du_i^{Na}}{dx_h}+\frac{d}{dx_h}(x_i^{Na})=\frac{du_i^{Nb}}{dx_h}+\frac{d}{dx_h}(x_i^{Nb})$$
$$\frac{dt_i^{Na}}{dx_h}+\frac{dt_i^{Nb}}{dx_h}=0\quad i=1,2 \tag{35}$$

Thus, the design sensitivity analysis is carried out by direct differentiation of the structural response [Eq. (27)] with respect to design variables:

$$\frac{\partial A}{\partial x_h}U+A\frac{\partial U}{\partial x_h}=\frac{\partial B}{\partial x_h}\Rightarrow A\frac{\partial U}{\partial x_h}=\left(\frac{\partial B}{\partial x_h}-\frac{\partial A}{\partial x_h}U\right) \tag{36}$$

This is a set of linear algebraic equations for the unknown gradients $\partial U/\partial x_h$ and equivalent to solving the same equation as Eq. (27). Thus, if the quantity in brackets in Eq. (36) is separately assembled, then the derivatives of displacements and tractions can be computed in one pass by reentering the equation solver. Following the calculation of displacement gradients, the gradients of stresses can be obtained [17].

The elastic compliance is evaluated as the strain energy of the structure:

$$E_s=\frac{1}{2}\int_s t_ju_j\,ds \tag{37}$$

The derivatives of the elastic compliance with respect to the boundary-point coordinate x_h can also be calculated analytically as follows:

$$\frac{\partial E_s}{\partial x_h}=\frac{1}{2}\left[\int_s\frac{\partial t_j}{\partial x_h}u_j\,ds+\int_s t_j\frac{\partial u_j}{\partial x_h}\,ds+\int_s u_jt_j\frac{\partial}{\partial x_h}\,ds\right] \tag{38}$$

Equation (38) shows that during the analysis, the compliance derivatives are calculated after the tractions, displacements, and their derivatives are obtained [18].

VI. Results and Discussion

The method presented here has been applied to several mode I and mixed-mode crack problems to compare its accuracy for different loading conditions and material properties. The engineering constants of the selected materials for the analysis are shown in Table 1. Every component is being treated as a lamina that has four engineering constants (E_1, E_2, G_{12}, and ν_{12}) with a lamina orientation angle of zero. When the fiber orientation is greater than zero, the equivalent engineering constants are determined and subsequently used in the analysis. Aluminium is an isotropic material, but in the current analysis, it is treated as if it is anisotropic [$E_1 = E_2$ and $G_{12} = 0.5 \cdot E_1(1 + \nu_{12})$]. In each case, the meshes were refined to ensure the convergence of the solution.

Five examples are analyzed and the results are presented as follows: a rectangular plate with a central crack subject to tensile stresses at the ends, a cantilever plate with a single edge crack loaded by shear stresses at its free end, a rectangular plate with a single edge crack or central slant crack subject to tension, and a circular arc crack in an infinite plate subject to equibiaxial tension (see Figs. 2–6, respectively).

The first example analyzed is an isotropic thin flat plate with a central crack of length $2a$ and width $2w$, subjected to tensile stresses

Table 1 Elastic properties of the selected materials

Material no.	Elastic properties	E_L, GPa	E_T, GPa	ν_{LT}, GPa	G_{LT}, GPa	Complex parameters μ_1	μ_2
1	Aluminium	70.0	70.0	0.3	26.923	i	i
2	Hypothetical $0.1 \le \phi \le 4.5$	$G_{LT}\cdot(\varphi+2\nu_{LT}+1.0)$	E_L/ϕ	0.03	6.0	i for $\phi=0.1$	$0.3162i$ for $\phi=0.1$
3	Graphite-epoxy	144.8	11.7	0.21	9.66	$0.951i$	$3.696i$
4	Glass-epoxy	48.26	17.24	0.29	6.89	$0.685i$	$2.440i$
5	Graphite-epoxy	138.9	8.96	0.3	7.1	$0.925i$	$4.255i$

σ at the ends of the plate, as shown in Fig. 2. Because of symmetric boundary conditions, only one-quarter of the plate needs to be analyzed. The BE mesh consists of 48 elements, and 40 elements were placed on the edge AB. The crack length is the only shape variable of this model. As explained in Sec. V, the shape variable is associated with the coordinates of a series of boundary nodes located on the crack surfaces, related to the boundary element discretization of the structure. If w in Eq. (29) is the crack length, then coordinates of each boundary point on the crack face are $x_i = \omega n_i$, where n_i is the fixed direction cosine at the boundary. Therefore, for each boundary point, $x_i' = \partial x_i/\partial\omega = n_i$.

Initially, the sensitivity of the elastic compliance with respect to the crack length extension, which is equal to the SERR or J_1, is determined. The plate is loaded in mode I. Therefore, $K_{\mathrm{II}} = 0$, and using Eq. (8), K_{I} can be obtained. Figure 7 shows the variation of the SERR with respect to the crack length a/w obtained numerically,

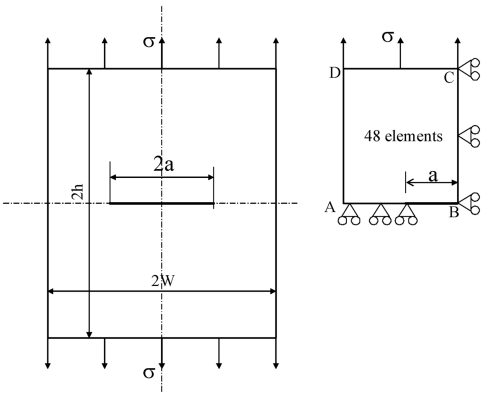

Fig. 2 Central crack in a rectangular plate subject to tension.

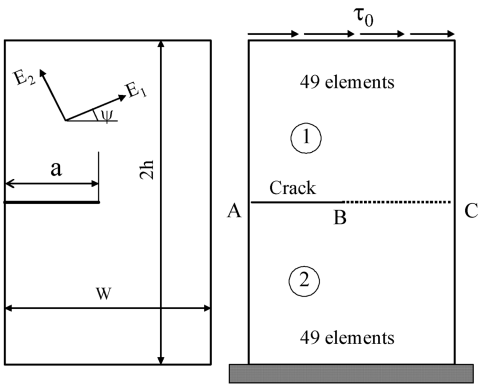

Fig. 3 Single edge crack in a cantilever plate loaded by shear stresses at its free end.

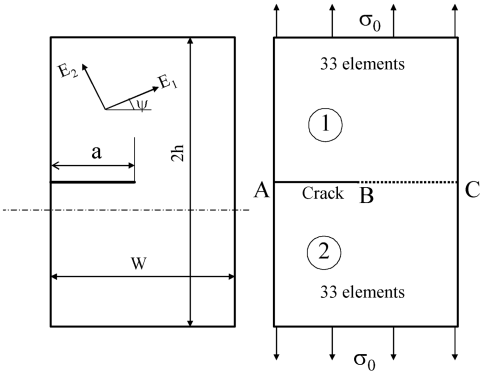

Fig. 4 Single edge crack in a rectangular plate subject to tensile stresses at the ends.

where a/w varies from 0.1 to 0.5. The corresponding SIF values are shown in Table 2.

There is an analytical solution for this example that gives K_{I} in terms of the normalized crack length a/w [28]:

$$K_{\mathrm{I}} = K_0 \frac{1 - (a/2w) + 0.326(a^2/w^2)}{\sqrt{1 - (a/w)}} \tag{39}$$

where $K_0 = \sigma\sqrt{\pi a}$. By substituting K_{I} from Eq. (39) into Eq. (12), the value of SERR can be obtained as follows:

$$J_1 = \frac{1}{E}\left(K_0 \frac{1 - (a/2w) + 0.326(a^2/w^2)}{\sqrt{1 - (a/w)}}\right)^2 \tag{40}$$

Table 2 shows the analytical values of K_{I} for different ratios of a/w obtained using Eq. (39). Figure 7 shows the variation of SERR with respect to a/w obtained using Eq. (40). It can be observed that the present numerical results are in very good agreement with the analytical solution.

Next, the same plate with a central crack but made of material no. 2 is analyzed, where $E_1 = G_{12}(\phi + 2\nu_{12} + 1)$, and the shear modulus G_{12} and Poisson's ratio ν_{12} have fixed values of 6 GPa and 0.03, respectively. The parameter $\phi = E_1/E_2$ varies from 0.1 to 4.5. The crack length-to-width ratios of $a/w = 0.2$, 0.5, and 0.8 are considered. This example was also studied by Bowie and Freeze [5], in which they used the modified mapping collocation technique, and by Sollero and Aliabadi [8], in which they employed the J integral in conjunction with the BEM. Here, with their SIFs [5,8] and using Eq. (13), the corresponding SERR values are calculated and compared with the SERR values obtained using the shape sensitivities.

Figures 8 and 9 show the variations of the normalized SIFs and the SERR of the plate with respect to the change of ϕ, respectively. It can

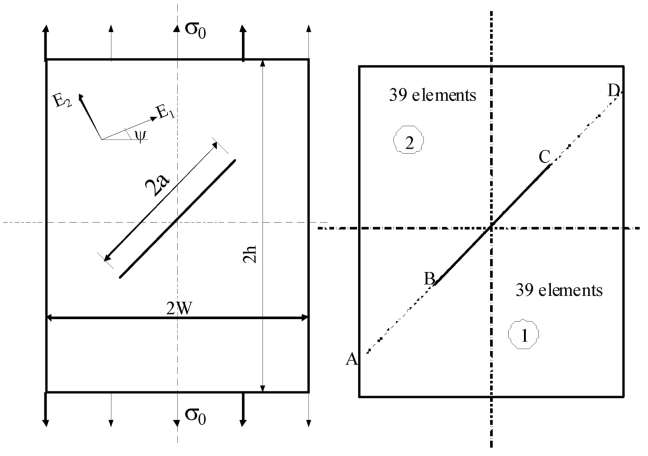

Fig. 5 Central slant crack in a rectangular plate subject to tension.

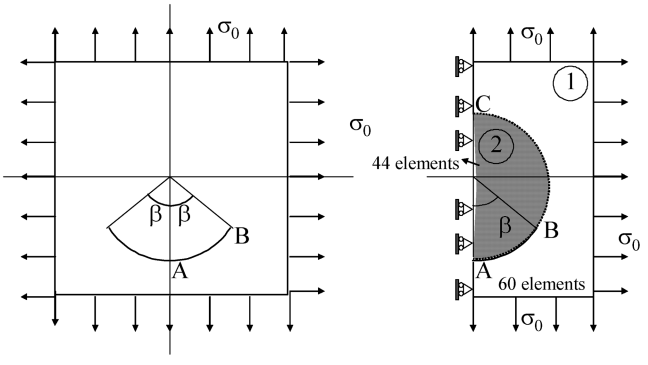

Fig. 6 A circular arc crack in an infinite plate subject to equibiaxial tension.

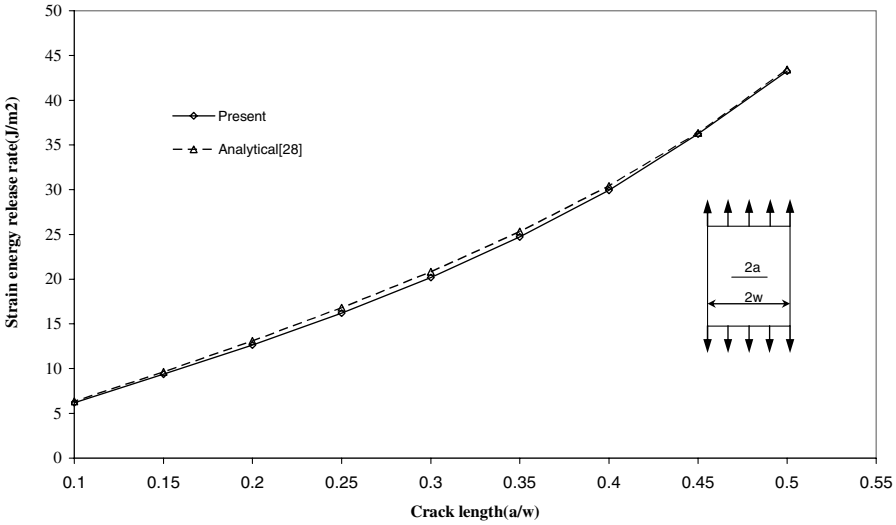

Fig. 7 Variation of stain energy release rate with respect to the crack length for the plate with a central crack subject to tension for material no. 1.

be observed that the present results are in very good agreement with the results published in [5,8]. However, for $a/w = 0.8$, when $\phi > 1.0$, there is a slight discrepancy in the SERR and SIF values obtained by Bowie and Freeze [5]. The results show that for a given crack length, when $\phi > 1.0$, the SERR and the SIFs are almost independent of the value of ϕ. For $\phi < 1$, as ϕ decreases, the SERR decreases, whereas the SIFs increase. This is due to the fact that the load is applied in the E_2 direction and ϕ is proportional to the invert of E_2.

The next example is a rectangular plate of width w with a single edge crack of $a/w = 0.5$. Material no. 3, which is graphite-epoxy, is selected for the analysis and the directions of fibers are rotated from $\psi = 0$ to 90 deg. The plate is divided into two subregions in which continuity of the traction and displacement along BC, according to Eqs. (28), is considered. The BE mesh of each region consists of 49 elements, of which 40 elements were placed on edge AC. Two types of loadings are studied. Figure 3 shows the plate clamped at one end and loaded by a uniform shear force of τ_0 at the free end. Figure 4 shows the same plate subject to tensile stresses σ at both ends.

Figure 10 shows the variation of normalized modes I and II SIFs with respect to the fiber orientation ψ for the cantilever plate subject to shear, where $K_0 = \tau_0\sqrt{\pi a}$. This example was also studied by Chu and Hong [6] and by Sollero and Aliabadi [8], in which they employed the J integral in conjunction with the FEM [6] or BEM [8], respectively. Their results are included in Fig. 10, which are in very good agreement with the present findings. Figure 11 shows the variation of SERR with respect to the fiber angle obtained from the present study and those calculated from the SIF values published in [6,8]. It can be seen that the present results are in very good agreement with those obtained by Sollero and Aliabadi [8]. However, for $\psi < 30$ deg, there is a slight discrepancy in the results produced by Chu and Hong [6]. It can be observed that there is a small variation of the normalized SIFs with respect to the fiber angle. K_I/K_0 changes from a minimum value of 8.67 to a maximum value of 9.42, whereas K_{II}/K_0 varies from 0.97 to 1.40. The variation of the SERR with respect to the fiber angle is more evident. For $\psi < 30$ deg, the SERR is almost independent of the fiber angle. For $\psi > 30$ deg, there is a sharp drop in the SERR, and the higher the fiber angle, the lower the SERR. For $\psi = 90$ deg, the SERR has the least value, as expected.

Table 2 Stress intensity factors for the plate with the central crack subject to tension for material no. 1

a/w	K_I/K_0 (present)	K_I/K_0 (analytical) [28]
0.1	1.00	1.00
0.15	1.01	1.01
0.2	1.01	1.02
0.25	1.03	1.03
0.3	1.05	1.05
0.35	1.07	1.07
0.4	1.1	1.10
0.45	1.14	1.13
0.5	1.19	1.17

Figure 12 shows the variation of the SERR with respect to the fiber angle when the plate is subjected to tension at its ends (Fig. 4). The corresponding normalized mode I SIFs of the plate are included in Fig. 10. It can be observed that for $\psi < 20$ deg, the SERR is almost independent of the fiber angle, and after a slight increase of SERR, when $20 \text{ deg} < \psi < 30$ deg, there is a sharp drop in the SERR. The SERR has the least value when the load is applied along the fiber direction ($\psi = 90$ deg), as expected.

For both loading cases, the normalized SIF values with isotropic material properties (material no. 1) are also obtained and presented in Fig. 10. It can be observed that for the cantilever plate, when $\psi < 60$ deg, K_{II} is almost independent of the material property of the cantilever plate. For the plate subject to tension, when $\psi > 30$ deg, K_I is almost independent of the material property of the plate.

It can be concluded that although the SIF is of fundamental importance for anisotropic materials in the prediction of brittle failure using linear elastic fracture mechanics, for composite laminates, the direct evaluation of the SERR would easily characterize their crack instability with respect to the fiber orientation.

The next example is a central slant crack of length $a/w = 0.2$ in a rectangular plate of height-to-width ratio of $h/w = 0.2$ subjected to tension(s). The crack is inclined with the angle of ϕ with respect to the plate sides and the fiber orientation varies from 0 to 120 deg, as shown in Fig. 5. The plate is divided into two subregions and the BE mesh of each region consists of 39 elements, of which 30 elements were placed on edge AD. The material is a glass-epoxy composite (material no. 4 in Table 1). Table 3 shows the normalized SIF values for the crack angle of $\phi = 45$ deg, where $K_0 = \sigma_0\sqrt{\pi a}$. The SIF values obtained by Sollero and Aliabadi [8] and Gandhi [2] are also presented in Table 3, which agree very well with the present results. Gandhi [2] used the modified mapping collocation technique. Figure 13 shows the variation of SERR with respect to the fiber orientation, obtained using the present method, and those computed from the SIF values reported in [2,8], which are in very good agreement.

To examine the effect of the crack orientation angle on the SERR and SIFs, the crack angles of $\phi = 0$, 30, and 60 deg were studied, for which the crack length was fixed at $a/w = 0.2$. For each crack direction, the fiber orientation varied from 0 to 120 deg. Figure 13 shows the variation of the SERR with respect to the fiber angle for different crack orientations. Figure 14 shows the variation of the SERR with respect to the crack orientation angle ϕ of the plate for different fiber orientations. The results show that for any crack orientation angle, the same trend of

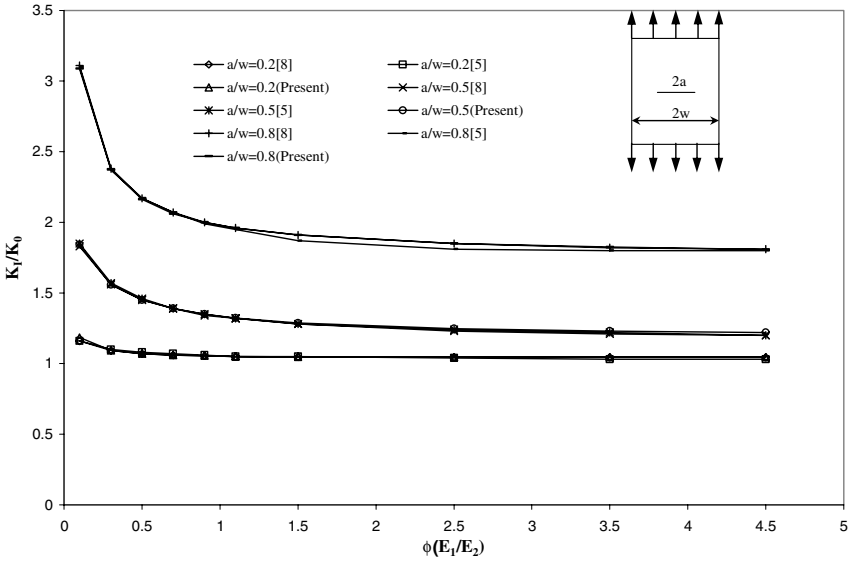

Fig. 8 Variation of stress intensity factor K_1/K_0 with respect to the change of $\phi(E_1/E_2)$ for the plate with different central crack lengths a/w subject to tension for material no. 2.

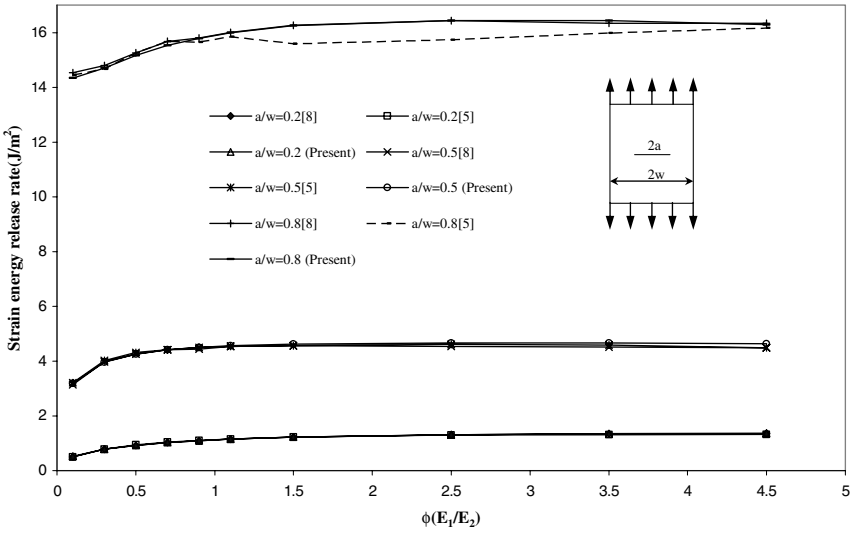

Fig. 9 Variation of strain energy release rate with respect to the change of $\phi(E_1/E_2)$ for the plate with different central crack lengths a/w subject to tension for material no. 2.

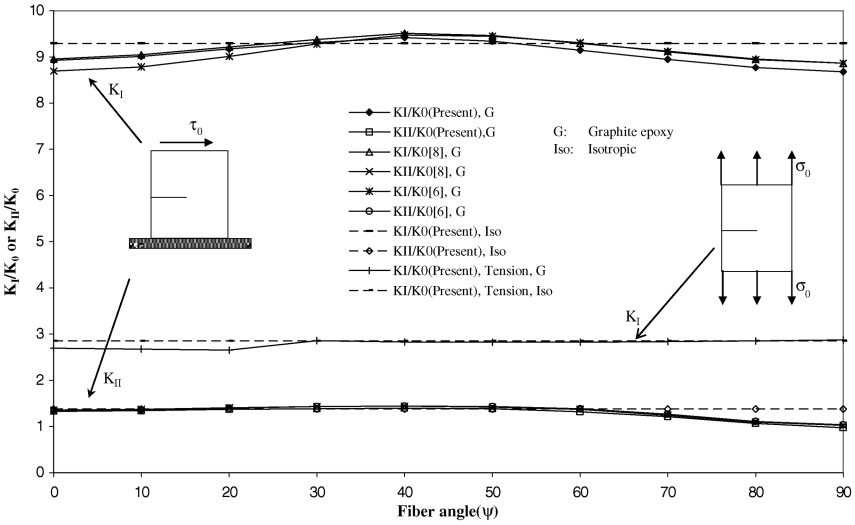

Fig. 10 Variation of the normalized stress intensity factors (K_I/K_0 or K_{II}/K_0) with respect to ψ for the rectangular plate with a single edge crack of $a/w = 0.5$ subject to tension or shear for material nos. 1 and 3.

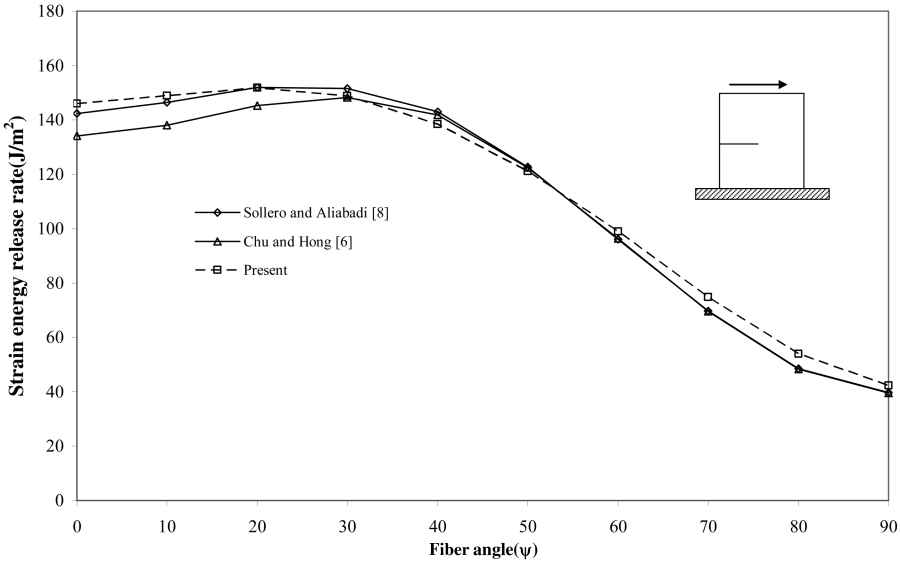

Fig. 11 Variation of strain energy release rate with respect to ψ for the rectangular plate with a single edge crack of $a/w = 0.5$ subject to shear for material no. 3.

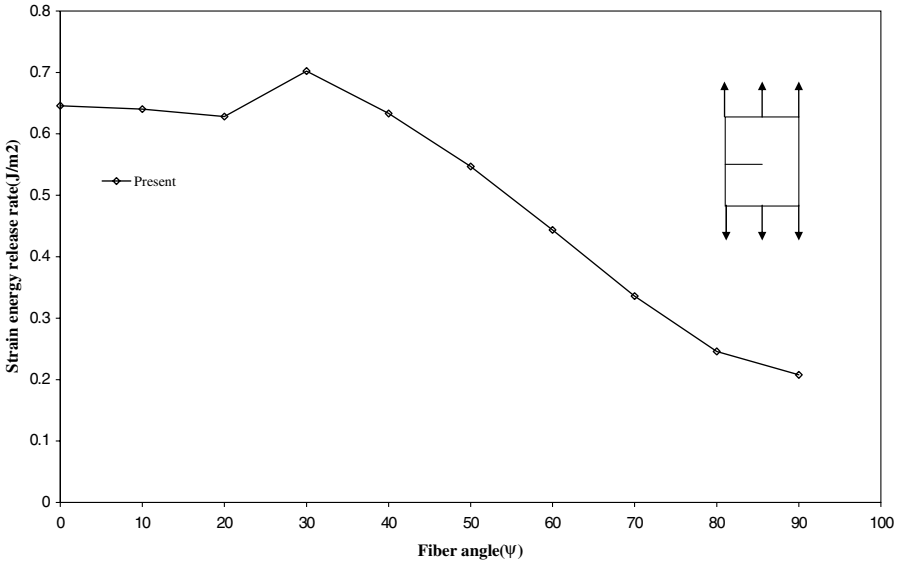

Fig. 12 Variation of strain energy release rate with respect to ψ for the rectangular plate with a single edge crack of $a/w = 0.5$ subject to tension for material no. 3.

variation for SERR, with respect to the fiber angle, can be observed. The minimum and maximum values of the SERR occur when the loads are applied in the fiber direction ($\psi = 90$ deg) and in the transverse direction of the fibers ($\psi = 0$), respectively For any fiber orientation angle, the maximum SERR occurs when the crack orientation angle is zero, and the higher the crack orientation angle, the lower the SERR. For any fiber orientation angle, the crack angle of $\phi = 60$ has the least value of SERR, and for this crack direction, the variation of the SERR with respect to the fiber angle is relatively small.

To apply the current method for the curved crack geometries, the problem of a crack with a circular arc shape in an unbounded domain is analyzed. Figure 6 shows a circular arc crack with the semi-angle of β in an infinite plate subject to uniform tension σ in two perpendicular directions. Material nos. 1 and 5, which are isotropic and graphite-epoxy, respectively, are considered for the analysis. Cracks with semi-angles of 10 to 90 deg, with an increment of 10 deg, are modeled and analyzed. The plate is divided into two subregions and the BE meshes of the regions consist of 60 and 44 elements, respectively, of which 36 elements were placed on each side of the semicircle edge ABC.

For the plate with isotropic material property (material no. 1), the normalized modes I and II SIF values are computed and compared with those results obtained by Chen [29] and Garcia et al. [9].

Table 3 Stress intensity factors for the plate with the central slant crack subject to tension for material no. 3 ($\phi = 45$ deg)

φ	K_I/K_0 (present)	K_{II}/K_0 (present)	K_I/K_0 [2]	K_{II}/K_0 [2]	K_I/K_0 [8]	K_{II}/K_0 [8]
0	0.5217	0.5082	0.5220	0.5070	0.5100	0.5000
45	0.5207	0.5147	0.5150	0.5050	0.5120	0.5080
90	0.5138	0.5089	0.5130	0.5090	0.5250	0.5070
105	0.5155	0.5101	0.5130	0.5100	0.5270	0.5040
120	0.5185	0.5127	0.5240	0.5120	0.5250	0.5020

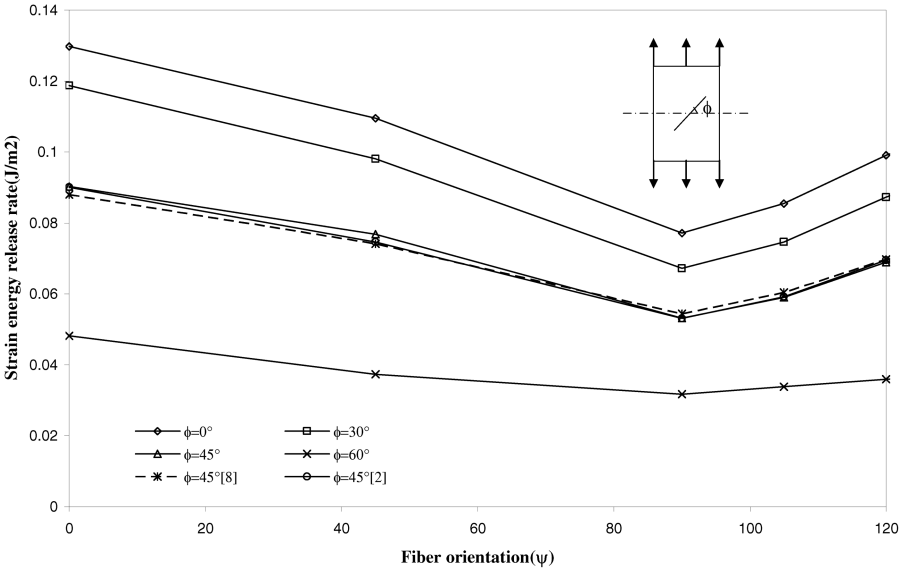

Fig. 13 Variation of strain energy release rate with respect to ψ for the plate with the central slant crack at different angles for material no. 4.

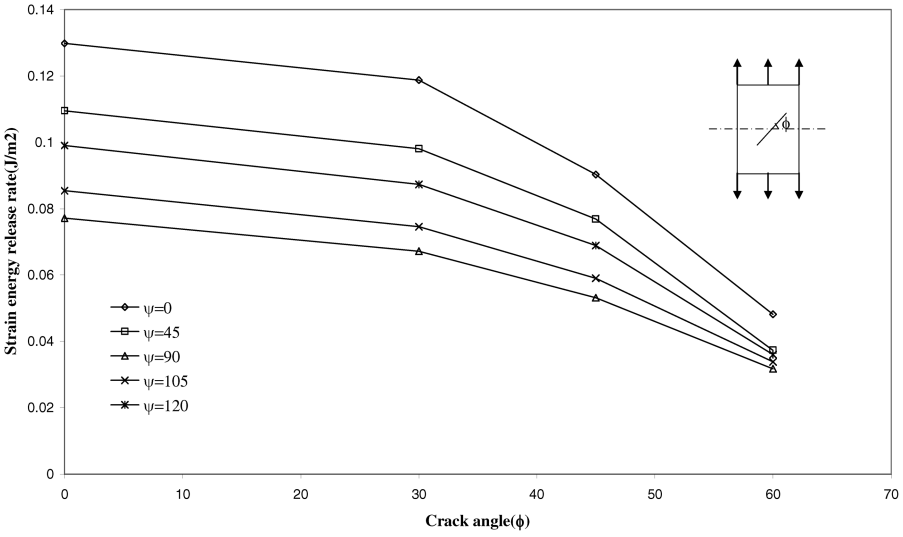

Fig. 14 Variation of the strain energy release rate with respect to ϕ for different fiber orientations for the plate with a central slant crack subject to tension for material no. 4.

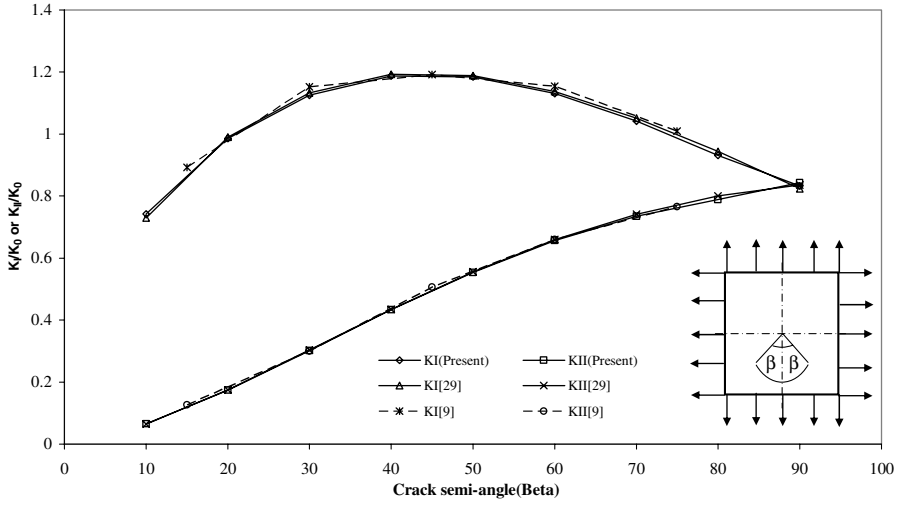

Fig. 15 Variation of the stress intensity factors with respect to the crack semi-angle for the isotropic plate with a circular crack subject to equibiaxial tensile stresses (material no. 1).

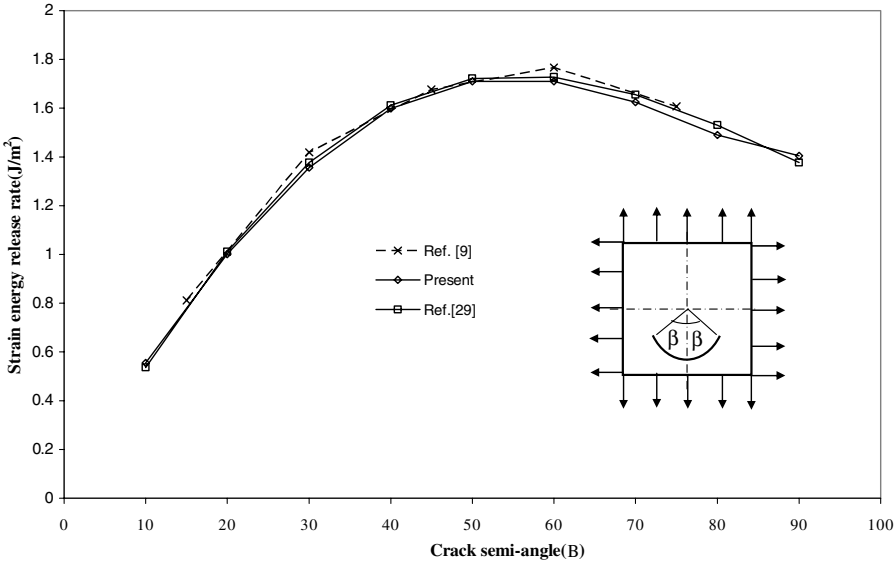

Fig. 16 Variation of the strain energy release rate with respect to the crack semi-angle for the isotropic plate with a circular crack subject to equibiaxial tensile stresses (material no. 1).

In [29], a singular integral equation was developed that contained the crack-opening displacement for solving plane elasticity problems. Chen [29] evaluated the SIFs for curved and kinked cracks in plane extension. In [9], a general mixed-mode boundary element approach for anisotropic media is presented in which integration of the singular and hypersingular kernels along quadratic line elements is carried out by analytical transformation of the integrals into regular integrals. Figure 15 shows the variations of the SIFs with respect to the crack semi-angle β using the present method and those obtained in [9,29], which are in very good agreement. Variation of the SERR with respect to the crack semi-angle is shown in Fig. 16. Using the SIFs in [9,29] and Eq. (17), the corresponding SERRs are evaluated and compared with the present findings. The results show that for the isotropic material, K_{II} has an almost linear variation with respect to the crack semi-angle and is at its maximum when the crack semi-angle is $\beta = 90$ deg. Figure 16 shows that the SERR has a nonlinear variation with respect to the crack semi-angle and the maximum SERR occurs when the crack semi-angle is between 55 and 65 deg. When $\beta < 55$ deg, the higher the crack angle, the higher the SERR, but when $\beta > 65$ deg, the higher the crack angle, the lower the SERR.

The curved crack with a circular arc shape in an unbounded domain is also analyzed with material no. 5, which is graphite-epoxy, for which the fiber angle is changing from $\psi = 0$ to 90 deg. Figure 17 shows the variation of the SERR with respect to the crack semi-angle for different fiber orientations of the graphite-epoxy plate. It can be observed that when fibers are in the y direction ($\psi = 90$ deg), the SERR has the lowest value for any crack orientation angle. It is shown that for $\psi = 90$ deg, SERR has an almost linear variation with respect to the crack semi-angle, and the higher the crack angle, the higher the SERR. For other fiber orientations, the variation of SERR with respect to the crack semi-angle is nonlinear where the maximum SERR occurs when 55 deg $< \beta <$ 65 deg. The SIF values of the plate with the fiber orientation of $\psi = 90$ deg for different crack angles are computed and compared with those obtained by Wang and Sun [10], in which they used integration by parts to the traditional boundary integral formulation for the analysis of the cracked 2-D anisotropic bodies. Figure 18 shows that their results are in very good agreement with the present findings.

Early application of the BEM involving interactions of multiple cracks and rigid lines representing fibers dates back to the 1990s [30–33]. The modeling of crack and fiber interactions is essential for a comprehensive model of damage in composites. However, the present study focuses on the crack analysis of a lamina at the macroscale, in which the equivalent engineering constants are used for the analysis. At present, the most common method used in the industry for the crack analysis is the J integral in conjunction with the FEM. The application of the J integral with the BEM will reduce the time of modeling and analysis but would still require the

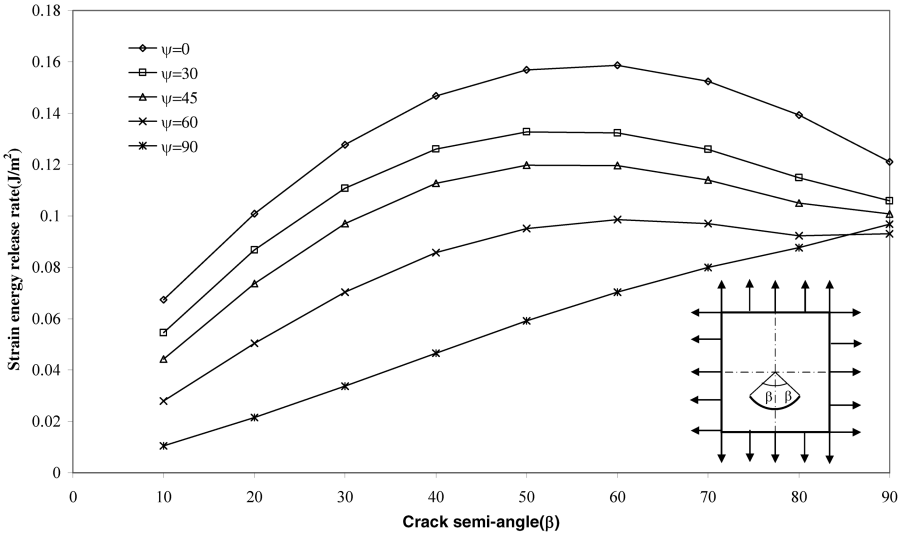

Fig. 17 Variation of the strain energy release rate with respect to the crack semi-angle for different fiber orientation of the graphite-epoxy plate (material no. 5).

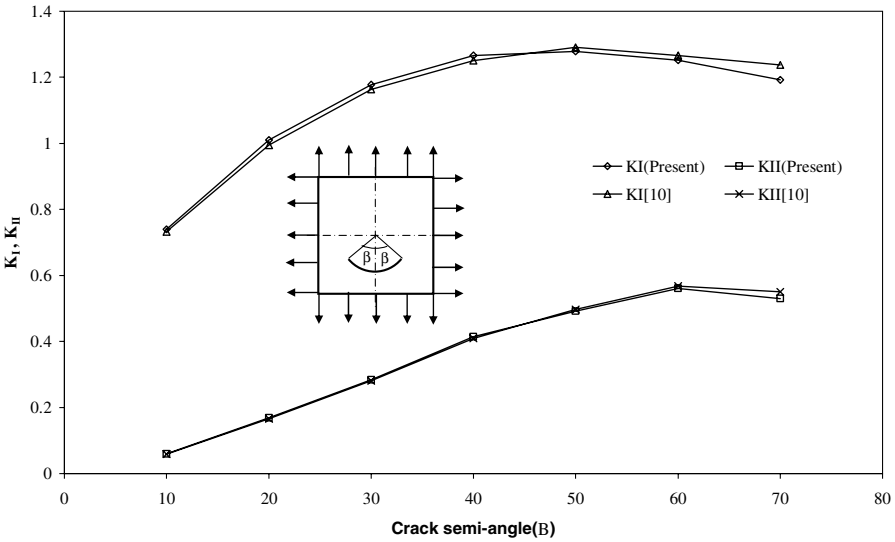

Fig. 18 Variation of the normalized stress intensity factors with respect to the crack semi-angle of a graphite-epoxy plate for the fiber angle of $\psi = 90$.

calculation of stresses and strains at a series of internal points around the crack for evaluation of the path-independent integrals. Using the boundary element shape sensitivities with the design variables that represent the crack surfaces, the computational efficiency will be greatly improved.

VII. Conclusions

Following a brief review of the mathematical basis of the BIE method for multiregion anisotropic materials, analytical differentiation of the BIE was carried out with respect to the positions of the boundary nodes. Shape design sensitivity analysis for an anisotropic multiregion domain was performed to compute the derivatives of displacements, stresses, elastic compliance, etc., with respect to changes of boundary-point coordinates. The crack length of arbitrary geometric shape was designated as the shape design variable. Then each shape variable was associated with the coordinates of a series of boundary nodes located on the crack surfaces. Thus, the relevant velocity terms were applied together in the sensitivity analysis with respect to that variable to determine the gradient of the total strain energy of the structure with respect to the crack length extension. In contrast to the J-integral method, which would require the computation of stresses and strains at a series of internal points around the crack for evaluation of the path-independent integrals, the fracture mechanics parameters are evaluated here by direct differentiation of the BIE. Therefore, for the same number of elements, not only is the accuracy of the present method very high, but, in terms of computational modeling and analysis, it is much more efficient.

The sensitivity analysis algorithm was validated using the test cases with known analytical solutions. Five example problems were analyzed and the results were presented. Five different anisotropic materials were employed for the analysis. The isotropic materials were treated as if they were anisotropic. The results show that although the SIF is of fundamental importance in the prediction of brittle failure using linear elastic fracture mechanics, for composite laminates, the direct evaluation of the SERR would easily characterize their crack instability with respect to the fiber orientation. The results show that the SERR was highly influenced by the fiber orientation of the composite lamina. Therefore, a laminate can be tailored to crack-growth resistance. Because of the flexibility of the present method, the future studies should cover the analysis of multiple curved cracks, kinked cracks, and bimaterial interface cracks in composites using the boundary element shape sensitivities.

References

[1] Snyder, M. D., and Cruse, T. A., "Boundary Integral Equation Analysis of Cracked Anisotropic Plates," *International Journal of Fracture*, Vol. 11, No. 2, Apr. 1975, pp. 315–28. doi:10.1007/BF00038898

[2] Gandhi, K. R., "Analysis of an Inclined Crack Centrally Placed in an Orthotropic Rectangular Plate," *Journal of Strain Analysis for Engineering Design*, Vol. 7, No. 3, 1972, pp. 157–162. doi:10.1243/03093247V073157

[3] Cruse, T. A., *Boundary Element Analysis in Computational Fracture Mechanics*, Kluwer, Dordrecht, The Netherlands, 1988.

[4] Hayes, D. J., "A Practical Application of Buekner's Formulation for Determining Stress Intensity Factors for Cracked Bodies," *International Journal of Fracture Mechanics*, Vol. 8, No. 2, 1972, pp. 157–165. doi:10.1007/BF00703877

[5] Bowie, O. L., and Freeze, C. E., "Central Crack in Plane Orthotropic Rectangular Sheet," *International Journal of Fracture Mechanics*, Vol. 8, No. 1, 1972, pp. 49–58. doi:10.1007/BF00185197

[6] Chu, S. J., and Hong, C. S., "Application of the J_k Integral to Mixed Mode Crack Problems for Anisotropic Composite Laminates," Vol. 35, No. 6, 1990, pp. 1093–1103.

[7] Tan, C. L., and Gao, Y. L., "Boundary Element Analysis of Plane Anisotropic Bodies with Stress Concentrations and Cracks," *Composite Structures*, Vol. 20, No. 1, 1992, pp. 17–28. doi:10.1016/0263-8223(92)90008-Z

[8] Sollero, P., and Aliabadi, M. H., "Fracture Mechanics Analysis of Anisotropic Plates By the Boundary Element Method," *International Journal of Fracture*, Vol. 64, No. 4, 1993, pp. 269–284. doi:10.1007/BF00017845

[9] Garcia, F., Saez, A., and Dominguez, J., "Traction Boundary Elements for Cracks in Anisotropic Solids," *Engineering Analysis with Boundary Elements*, Vol. 28, No. 6, 2004, pp. 667–676. doi:10.1016/j.enganabound.2003.08.005

[10] Wang, Y. B., and Sun, Y. Z., "A New Boundary Integral Equation Method for Cracked 2-D Anisotropic Bodies," *Engineering Fracture Mechanics*, Vol. 72, No. 13, 2005, pp. 2128–2143. doi:10.1016/j.engfracmech.2005.01.007

[11] Chang, J. H., and Wu, D. J., "Computation of Mixed-Mode Stress Intensity Factors for Curved Cracks in Anisotropic Elastic Solids," *Engineering Fracture Mechanics*, Vol. 74, No. 8, 2007, pp. 1360–1372. doi:10.1016/j.engfracmech.2005.07.011

[12] Parker, A. P., "The Mechanics of Fracture and Fatigue," E. & F.N. Spon, Ltd, New York, 1981.

[13] Rice, J. R., "A Path Independent Integral and the Approximate Analysis of Strain Concentration by Notches and Cracks," *Journal of Applied Mechanics*, Vol. 35, 1968, pp. 379–386.

[14] Keum, D. J., and Kwak, B. M., "Calculation of Stress Intensity Factors by Sensitivity Analysis with Respect to Change of Boundary Conditions," *Computers and Structures*, Vol. 44, Nos. 1–2, 1992, pp. 63–69. doi:10.1016/0045-7949(92)90223-M

[15] Lee, T. W., and Grosse, J. R., "Energy Release Rate by a Shape Design Sensitivity Approach," *Engineering Fracture Mechanics*, Vol. 44, No. 5, 1993, pp. 807–819. doi:10.1016/0013-7944(93)90207-9

[16] Reddy, R. M., and Rao, B. N., "Continuum Shape Sensitivity Analysis of Mixed-Mode Fracture Using Fractal Finite Element Method," *Engineering Fracture Mechanics*, Vol. 75, No. 10, 2008, pp. 2860–2906.
doi:10.1016/j.engfracmech.2008.01.001

[17] Tafreshi, A., "Shape Design Sensitivity Analysis of 2-D Anisotropic Structures Using the Boundary Element Method," *Engineering Analysis with Boundary Elements*, Vol. 26, No. 3, 2002, pp. 237–251.
doi:10.1016/S0955-7997(01)00098-4

[18] Tafreshi, A., "Optimum Shape Design of Composite Structures Using the Boundary Element Method," *AIAA Journal*, Vol. 43, No. 6, 2005, pp. 1349–1359.
doi:10.2514/1.11502

[19] Tafreshi, A., "Shape Design Sensitivity Analysis with Respect to the Positioning of Features in Composite Structures Using the Boundary Element Method," *Engineering Analysis with Boundary Elements*, Vol. 30, No. 1, 2006, pp. 1–13.
doi:10.1016/j.enganabound.2005.08.003

[20] Tafreshi, A., "Shape Sensitivity Analysis of Composites in Contact Using the Boundary Element Method," *Engineering Analysis with Boundary Elements*, Vol. 33, No. 2, 2009, pp. 215–224.
doi:10.1016/j.enganabound.2008.04.008

[21] Tafreshi, A., "Efficient Modelling of Delamination in Composite Cylindrical Shells Under Axial Compression," *Composite Structures*, Vol. 64, Nos. 3–4, 2004, pp. 511–520.
doi:10.1016/j.compstruct.2003.09.050

[22] Tafreshi, A., "Instability of Delaminated Composite Cylindrical Shells Under Combined Axial Compression and Bending," *Composite Structures*, Vol. 82, No. 3, 2008, pp. 422–433.
doi:10.1016/j.compstruct.2007.01.021

[23] Tafreshi, A., "Delamination Buckling of Composite Cylindrical Shells," *Delamination Buckling of Composites*, edited by S. Sridharan, Woodhead, Cambridge, England, U.K., 2008, Chap. 20.

[24] Gibson, R. F., *Principles of Composite Material Mechanics*, McGraw–Hill, New York, 1994.

[25] Lekhnitskii, S. G., *Theory of Elasticity of an Anisotropic Elastic Body*, Holden-Day, San Fransisco, 1963.

[26] Blandford, G. E., Ingraffea, A. R., and Liggett, "Two-Dimensional Stress Intensity Factor Computations Using the Boundary Element Method," *International Journal for Numerical Methods in Engineering*, Vol. 17, No. 3, 1981, pp. 387–404.
doi:10.1002/nme.1620170308

[27] Tafreshi, A., and Fenner, R. T., "Design Optimization Using the Boundary Element Method," *Journal of Strain Analysis for Engineering Design*, Vol. 26, No. 4, 1991, pp. 231–241.
doi:10.1243/03093247V264231

[28] Solecki, R., and Conant, R. J., *Advanced Mechanics of Materials*, Oxford Univ. Press, Oxford, 2003.

[29] Chen, Y. Z., "Stress Intensity Factors for Curved and Kinked Cracks in Plane Extension," *Theoretical and Applied Fracture Mechanics*, Vol. 31, No. 3, 1999, pp. 223–232.
doi:10.1016/S0167-8442(99)00016-6

[30] Hu, K. X., Chandra, A., and Huang, Y., "On Interacting Bridged-Crack Systems," *International Journal of Solids and Structures*, Vol. 31, No. 5, 1994, pp. 599–611.
doi:10.1016/0020-7683(94)90140-6

[31] Chandra, A., Hu, K. X., and Huang, Y., "A Hybrid BEM Formulation for Multiple Cracks in Orthotropic Elastic Components," *Computers and Structures*, Vol. 56, No. 5, 1995, pp. 785–797.
doi:10.1016/0045-7949(95)00008-5

[32] Jiang, Z. Q., Chandra, A., and Huang, Y., "A Hybrid Micro-Macro BEM with Micro-Scale Inclusion-Crack Interactions," *International Journal of Solids and Structures*, Vol. 33, No. 16, 1996, pp. 2309–2329.
doi:10.1016/0020-7683(95)00155-7

[33] Huang, Y., Chandra, A., Wei, X., Jiang, Z. Q., and Hu, K. X., "A Numerical Calculation of Two-Dimensional Moduli for Microcracked Solids," *International Journal of Solids and Structures*, Vol. 33, No. 11, 1996, pp. 1575–1586.
doi:10.1016/0020-7683(95)00110-7

A. Roy
Associate Editor